Conformational characteristics of regioselectively PEG/PS-grafted cellulosic bottlebrushes in solution: cross-sectional structure and main-chain stiffness

Yuji Kinose,[1] *Keita Sakakibara,*[2] *and Yoshinobu Tsujii* [1,*]

[1]Institute for Chemical Research, Kyoto University, Gokasho, Uji, Kyoto 611-0011, Japan

[2]Research Institute for Sustainable Chemistry, National Institute of Advanced Science and Technology (AIST), 3-11-32 Kagamiyama, Higashihiroshima, Hiroshima 739-0046, Japan

RUNNING HEAD: Conformation of PEG/PS-grafted cellulosic bottlebrush

KEYWORDS: Cellulose, Regioselective grafting, Heterografted bottlebrush, SEC-MALS, SAXS, Kratky–Porod worm-like chain, Cross-sectional structure

Abstract

Cellulosic bottlebrushes with polystyrene (PS) and poly(ethylene glycol) (PEG) side chains at the *O*-6 and *O*-2,3 positions, respectively (PEG-PS-cellulose), were synthesized and characterized in diluted solution to reveal the second structure of heterografted bottlebrushes. The regioselectivity and degree of substitution were evaluated by ^{1}H- and ^{13}C-nuclear magnetic resonance spectroscopy and size-exclusion chromatography (SEC). The cross-sectional structure of PEG-PS-cellulose was evaluated from the cross-sectional radius of gyration determined by the small angle X-ray scattering technique as a function of the molecular weight of the PS side chain. As a result, PEG-PS-cellulose was found to show a core-shell-corona structure, in which PEG and PS side chains formed a homogeneous shell layer surrounding the cellulosic core and the longer PS chains formed an outer corona layer. The stiffness parameter (λ^{-1}) of the main chain was analyzed by the SEC–multiangle light scattering technique along with the Kratky-Porod wormlike chain model. In comparison with a previously reported cellulosic bottlebrush with a PS side chain at the *O*-6 position, it is suggested that the observed increase in λ^{-1} with increasing molecular weight of PS is mainly derived from the interaction among PS side chains located in an outer layer, while the PEG side chains at the *O*-2,3 position effectively suppressed the internal rotation of the cellulosic main chain.

Introduction

Graft polymers with highly dense side chains are known as bottlebrush polymers.[1] The main chain is stiffened by the excluded volume effect among the dense side chains with a liquid crystal phase formed in a dense solution in some cases.[2] Because of suppression of inter- and intramolecular entanglement of main chains, bottlebrushes attract attention as base materials for high-performance elastomers[3] and as pillars for porous materials.[4] Additionally, since a dense group of side chains can have characteristics equivalent to a polymer brush densely grafted onto a solid surface, i.e., a concentrated polymer brush, bottlebrushes are expected to as act as novel surface modifiers with desirable functionalities such as low friction, biocompatibility and a low anchoring coefficient for liquid crystals,[5,6,7,8] and they are regarded as an increasingly fascinating material. To distinguish between a bottlebrush with two types of side chains, as mentioned below, a bottlebrush with only one kind of side chain is called a homografted bottlebrush (homoBB) in this article.

Recent advances in precision polymer synthesis have led to the realization of a new type of bottlebrush possessing two or more types of side chains.[1] A bottlebrush that has different side chains introduced segmentally along the main chain is called a “block” type since different bottlebrushes are regarded to be connected in series. The bottlebrushes possessing two types of side chains uniformly grafted along the main chain (heterografted bottlebrush; heteroBB) are set

in the categories of the “Janus” type wherein the side chains undergo intramolecular phase separation around the main chain.[9,10] The Janus bottlebrush can act as a highly effective surfactant with a low critical micelle concentration because of its large interfacial area between immiscible side chains.[11,12] Meanwhile, the Janus bottlebrush can easily self-assemble into micelles[13] or vesicles[14,15] in solution, the shape of which is influenced by the curvature, and, hence, the main-chain stiffness of bottlebrushes. The distinct feature of a Janus bottlebrush is that the abovementioned configurational characteristics with a large interfacial area inside contribute to low entropy loss in forming microphase-separated structures, achieving a smaller domain pitch than conventional diblock copolymers with the same chemical composition.[16,17] Additionally, the stiffened main chain enables the reduction of entanglement, leading to the rapid progression of microphase separation. Thus, it is important to determine the secondary structure of heteroBBs.

To date, the secondary structures of heteroBBs in solution have been theoretically[18] and computationally[19,20,21] studied. For heteroBBs with a rigid main chain, it has been reported that the lower the affinity between solvent and side chains, the greater the intramolecular phase separation proceeds to change to the “Janus state” (i).[19] Additionally, in a poor or selective solvent for side chains, it has been predicted that heteroBBs with a stiff main chain and low-density or sparse side chains form a pearl-necklace structure (ii),[20] and that heteroBBs with a flexible main chain can form an intramolecular spherical aggregation (iii).[21] However, experimental studies on

the secondary structure of heteroBBs have not been sufficiently reported.

To clarify this issue and control the side- and main-chain conformation of bottlebrushes in solution, we focused on the use of cellulose as the main chain.[22,23] Cellulose is the major component of abundant plant biomass and has a chiral and stiff main chain. It possesses three kinds of hydroxy groups per repeat unit (anhydroglucose unit; AGU). Previously, we studied the conformation of the cellulose bottlebrush possessing a polystyrene (PS) chain at the *O*-6 position (PS-cellulose, **3**; see Figure 1) in a poor solvent for PS (*N*,*N*-dimethylformamide; DMF), revealing that it can maintain a semirigid, wormlike conformation because of the original stiffness of the cellulose even though an attractive interaction between side chains can otherwise lead to a "collapsed brush"[24] state. Thus, it is advantageous that a heteroBB is designed based on PS-cellulose to study its intramolecular phase separation (forming a Janus cylinder) as a function of a wide range of structural parameters and solvents without peal-necklace and intramolecular globule states in a dilute solution.

In this study, we prepared cellulosic bottlebrushes (PEG-PS-cellulose, **1**; see Figure 1) with PS and poly(ethylene glycol) (PEG) chains, a pair of which has a large Flory-Huggins interaction parameter χ,[25] at the *O*-6 and *O*-2,3 positions, respectively, as well as its precursor (PEG-cellulose, **2**; see Figure 1)[26], and analyzed their cross-sectional structure and main-chain stiffness in a selectively poor solvent. PS and PEG side chains were introduced by the stepwise

grafting-to method and monitored by size-exclusion chromatography (SEC), and the regioselectivity and degree of substitution (*DS*) were evaluated by ^{1}H- and ^{13}C-NMR. Small-angle X-ray scattering (SAXS) and SEC with multiangle light scattering detection (SEC-MALS) measurements were conducted in a poor solvent for the PS chain (DMF/LiBr). The cross-sectional structure around the main chain was discussed based on the data obtained for the cross-sectional mean squared radius of gyration ($\langle S_c^2 \rangle$) under the cross-sectional Guinier approximation[27] for SAXS profiles as a function of the molecular weight of the PS side chain using several cross-sectional models. The stiffness parameter (λ^{-1}) of the main chain was evaluated by analyzing the dependence of the mean squared radius of gyration ($\langle S^2 \rangle$) on the degree of polymerization of the main chain (DP_M) with the Kratky-Porod wormlike (KP) chain model.[28] Then, the effects of the PS- and PEG-side chains on λ^{-1} were discussed in comparison with previous studies on PS-cellulose, **3**.

Experimental Procedure

Measurements

Nuclear magnetic resonance (NMR) spectra (600 MHz and 800 MHz) were obtained using an AVANCE III 600 or AVANCE III 800 system (Bruker, MA, USA) with $CDCl_3$ or $C_2D_2Cl_4$. ^{13}C resonances were assigned with reference to a previously reported combination of heteronuclear single quantum correlation (HSQC) and ^1H-detected multiple bond coherence (HMBC) spectra.[26] SEC analysis was conducted with a Shodex GPC-101 system (Showa Denko K.K., Tokyo, Japan) equipped with a KF-G (Shodex) guard column, two KF-806 (Shodex) columns, and an RI-101 differential refractometer (Shodex) at a flow rate of 0.8 $mL \cdot min^{-1}$ at 40 °C. The eluent was tetrahydrofuran (THF), and the system was calibrated using standard samples of poly(methyl methacrylate) (PMMA). SEC-MALS analysis was conducted using a DAWN HELEOS II instrument (Wyatt Technology, Corp., Santa Barbara, CA, USA, $\lambda = 658$ nm) at room temperature (for MALS) combined with the abovementioned Shodex GPC-101 system, except that DMF with LiBr (10 mM) was used as the eluent. The click reaction was monitored by a Tosoh SEC system equipped with a CCPS pump (Tosoh Corp., Tokyo, Japan), KF-G guard column (Shodex), two KF-806L columns (Shodex), a CO-8020 column oven (Tosoh) at 40 °C, and a UV-8020 UV detector (Tosoh). THF with triethylamine (0.5 v%) was used as the eluent at a flow rate of 0.8 $mL \cdot min^{-1}$.

To determine the absolute values for the molecular weights from the SEC-MALS data, the refractive index increment (dn/dc) for **1** ((dn/dc)$_1$) was calculated using the following equation:[29]

$$\left(\frac{\mathrm{d}n}{\mathrm{d}c}\right)_{\mathbf{1}} = \left(\frac{\mathrm{d}n}{\mathrm{d}c}\right)_{\mathrm{PEG}} w_{\mathrm{PEG}} + \left(\frac{\mathrm{d}n}{\mathrm{d}c}\right)_{\mathrm{PS}} w_{\mathrm{PS}} + \left(\frac{\mathrm{d}n}{\mathrm{d}c}\right)_{\mathrm{EC}} (1 - w_{\mathrm{PEG}} - w_{\mathrm{PS}}) \qquad (1)$$

where (dn/dc)$_{\mathrm{PEG}}$, (dn/dc)$_{\mathrm{PS}}$, and (dn/dc)$_{\mathrm{EC}}$ are the refractive index increments for PEG, PS and ethyl cellulose (EC) homopolymers, respectively, and w_{PEG} and w_{PS} are the weight fractions of PEG and PS in bottlebrush **1**, respectively. Instead of the dn/dc value for unsubstituted cellulose, the value for EC was used as the main chain because unsubstituted cellulose did not dissolve in DMF/LiBr. The values of (dn/dc)$_{\mathrm{PEG}}$, (dn/dc)$_{\mathrm{PS}}$, and (dn/dc)$_{\mathrm{EC}}$ were measured to be 0.047 mL·g^{-1}, 0.158 mL·g^{-1}, and 0.045 mL·g^{-1}, respectively, using a differential refractometer (Optilab rEX, Wyatt Technology, λ = 658 nm, at 25 °C).

SAXS measurements were carried out at room temperature using a BL40B2 (at SPring-8, Hyogo, Japan) utilizing an imaging plate (RIGAKU R-AXIS VII) and a flat cell (width, 3 mm) with a pair of thin quartz glass windows (thickness, 20 μm) under the conditions of an X-ray wavelength of 1.000 Å and a camera length of 1654 mm; further details are given in the reference.[22] The excess scattering intensity $I(q)$ for the solutions of the bottlebrushes with a concentration of 0.5% w/v in DMF/LiBr was obtained from the difference in the scattering intensity of the solvent.

Synthesis

Regioselective synthesis of bottlebrushes **1** and **2** in part (scheme 1) has been reported previously[26] and slightly modified in this study. Commercial chemicals were of the highest grade available and used without further purification. All reactions requiring nonaqueous conditions were conducted in oven-dried glassware under an Ar atmosphere. The starting material, 6-*O*-*p*-methoxytritylcellulose (MeOTr-cellulose, **4**), was synthesized from microcrystalline cellulose (MCC) (1.02331.0500, Merck, Germany) according to Gömez et al.[30] The degree of substitution (*DS*) of the *p*-methoxytrityl (MeOTr) group was estimated to be 1.06 based on elemental analysis. Methoxy poly(ethylene glycol) iodide (PEG-I) (MW = 860 g·mol^{-1}, DP_n = 16) was synthesized from monomethoxy poly(ethylene glycol) (MeO-PEG) (MW = 750 g·mol^{-1}, Sigma–Aldrich, US) according to Yue et al.[31] Azido-terminated PS (PS-N_3) was synthesized via atom transfer radical polymerization followed by a substitution reaction according to Matyjaszewski et al.[32] The number-average molecular weight (M_n) and dispersity ($Đ$) of PS-N_3 were 6.4×10^3 g·mol^{-1} and 1.1, 3.3×10^3 g·mol^{-1} and 1.1, 2.2×10^3 g·mol^{-1} and 1.1 for the synthesis of **1a**, **1b**, **1c,** respectively. The percentage of azidation of PS-N_3 was estimated from the ^{1}H-NMR spectrum to be over 90%.

6-*O*-MeOTr-2,3-di-*O*-PEG_{16}-cellulose (**5**) was synthesized according to a previously reported method with modification.[31] NaOH (3.35 g, 83.7 mmol) was added to the solution of **4** (1.90 g, 4.37 mmol per AGU) in anhydrous dimethyl sulfoxide (DMSO) (57 mL). After 3 h, one-

half of the solution of PEG-I (DP_n = 16; 71.1 g, 82.7 mmol) in anhydrous DMSO (38 mL) was added dropwise over 40 min at room temperature, followed by stirring at 50 °C for 1 day. Then, another half of the PEG-I solution was added over 30 min into the reaction mixture and stirred for 3 h at 50 °C. The reaction mixture was extracted with CH_2Cl_2 (200 mL) and washed with distilled water (5 times), and then, the organic phase was dried over Na_2SO_4 and concentrated to yield the crude product. The crude product was purified by 10 reprecipitations from CH_2Cl_2 to a mixture of ethyl acetate and hexane (1:3 v/v). The final precipitate obtained was dried in a vacuum oven to yield **5** (5.20 g, 75%). SEC: $M_w = 1.9\times10^5$ g·mol^{-1}, $Đ = 2.2$. ^{1}H NMR (600 MHz, $CDCl_3$): 2.5-5.0 (-O-CH_2-, -Ph-O-CH_3, ring-H), 3.38 (-CH_2-O-CH_3), 3.55 (-CH_2-O-CH_3), 6.0-8.5 (-Ph).

2,3-Di-*O*-PEG$_{16}$-cellulose (**6**) was synthesized according to a method reported previously with modification.[30] **5** (4.50 g, 2.84 mmol per AGU) was dissolved in THF (180 mL), and aqueous HCl (35%, 9.0 mL) was added to the solution and stirred at room temperature for 5 h. The reaction mixture was neutralized with triethylamine and concentrated. The sticky mixture was dissolved in CH_2Cl_2 (100 mL) and washed with distilled water (four times), and the organic phase was dried over Na_2SO_4 and concentrated to yield the crude product. This crude product was added to distilled water, and the precipitate was removed by centrifugation. The supernatant fluid was filtered and dried under vacuum to yield **6** (3.27 g, 88%). SEC: $M_w = 1.1\times10^5$ g·mol^{-1}, $Đ$ =

1.9. ^{1}H NMR (600 MHz, $CDCl_3$): 2.6-5.0 (-O-CH_2-, ring-H), 3.38 (-O-CH_3), 3.55 (-CH_2-O-CH_3). DS_{PEG} (calculated from ^{1}H-NMR spectrum) = 1.6.

6-*O*-Pentynoyl-2,3-di-*O*-PEG_{16}-cellulose (PEG-cellulose, **2**) was synthesized as follows: 1-Ethyl-3-(3-dimethylaminopropyl)carbodiimide hydrochloride (EDC•HCl) (0.962 g, 5.02 mmol), pentynoic acid (0.328 g, 3.34 mmol), and 4-dimethylaminopyridine (0.615 g, 5.03 mmol) were added to a solution of **6** (1.00 g, 0.746 mmol per AGU) in anhydrous dimethylformamide (DMF) (20 mL). The mixture was stirred for 1 d at room temperature and stirred for 2 d at 50 °C. The reaction mixture was diluted with distilled water, dialyzed with a dialysis membrane (MWCO: 8 kD) for 1 d, and lyophilized to yield **2** (1.04 g, quant.). SEC: M_w = 6.2×10^4 g·mol^{-1}, $Đ$ = 1.5. ^{1}H NMR (800 MHz, 80 °C, $C_2D_2Cl_4$): 2.15 (-C≡CH), 2.55 (-CH_2-CH_2-C≡CH), 2.61 (-CH_2-C≡CH), 3.39 (3H, s, -CH_2-O-CH_3), 3.56 (3H, s, -CH_2-O-CH_3), 3.4-3.8 (-CH_2-), 2.8-5.5 (ring-H). ^{13}C NMR (800 MHz, 80 °C, $C_2D_2Cl_4$): 14.2 (-*C*H_2-C≡CH), 33.3 (-*C*H_2-CH_2-C≡CH), 58.6 (-O-CH_3), 62.9 (C6), 69.8 (-C≡*C*H), 69-71 (-O-CH_2-), 71.1-73.2 (C5), 71.8 (-*C*H_2-O-CH_3), 78.1 (C4), 82.0 (C2), 82.9 (-*C*≡CH), 83.2 (C3), 102.6 (C1), 170.9 (C=O). $DS_{pentynoyl}$ (calculated from ^{1}H-NMR spectrum) = 1.0.

2,3-Di-*O*-PEG_{16}-6-*O*-PS-cellulose (PEG-PS-cellulose, **1**) was obtained by the reaction of **2** with PS-N_3 in DMF as follows: Ascorbic acid (57.4 mg, 0.326 mmol) and copper(II) sulfate pentahydrate ($CuSO_4$•$5H_2O$) (8.0 mg, 0.032 mmol) were added to a solution of **2** (50.0 mg, 0.0358

mmol per AGU) in DMF (4.4 mL), PS-N_3 (M_n = 6.4×10^3 g·mol^{-1}, *DP* = 60; 376 mg, 0.0585 mmol) under an Ar atmosphere, and the solution was stirred at 60 °C for 2 d. The reaction mixture was passed through an alumina column and dried under vacuum to yield a brown crude product, which was dissolved in CH_2Cl_2 (1 mL). The solution was poured into a mixture of hexane and cyclohexane (3:2, v/v), and the precipitate was collected by centrifugation. This procedure was repeated twice, and the final product was dried under vacuum at 60 °C for 6 h to yield **1a** (216 mg, 75%). SEC-MALS: M_w = 9.7×10^5 g·mol^{-1}, $Đ$ = 2.3. ^{1}H NMR (600 MHz, $CDCl_3$): 0.8-1.1 (-CH_2-CH_3, -C-$(CH_3)_2$), 1.2-2.5 (-CH_2-C*H*Ph-), 2.5-5.5 (-O-CH_2-, ring H, -N-C*H*(Ph)-CH_2-), 3.38 (-O-CH_3), 3.55 (-CH_2-O-CH_3), 6.2-7.5 (arom-H, N-C*H*=C). Similarly, PEG-PS-cellulose with different *DP*s for PS, **1b** and **1c**, was prepared by the reaction of **2** (100 mg, 0.0715 mmol per AGU; 150 mg, 0.107 mmol per AGU) with PS-N_3 with different *DP*s (M_n = 3.3×10^3 g·mol^{-1}, *DP* = 30, 392 mg, 0.117 mmol; M_n = 2.2×10^3 g·mol^{-1}, *DP* = 20, 397 mg, 0.175 mmol) in the presence of ascorbic acid (114 mg, 0.648 mmol; 173 mg, 0.980 mmol) and $CuSO_4$•$5H_2O$ (16.2 mg, 0.0648 mmol; 24.4 mg, 0.0977 mmol) in DMF (8.6 mL; 13 mL), respectively. Yield: **1b**, 76% and **1c**, 75%. SEC-MALS: **1b**, M_w = 6.1×10^5 g·mol^{-1}, $Đ$ = 2.4 and **1c**, M_w = 4.8×10^5 g·mol^{-1}, $Đ$ = 2.4.

Results and Discussion

Regioselective synthesis of PEG-PS-cellulose 1a–c and PEG-cellulose 2

Regioselective synthesis of bottlebrushes **1** and **2** in part (Scheme 1) has been reported previously,[26] and a detailed characterization is given. First, to yield **6**, successful esterification of the residual hydroxy groups of **4** with PEG-I followed by complete deprotection of the MeOTr group with HCl was confirmed using the ^{1}H NMR spectrum of **6** (Figure S1): the peak derived from the methylene of PEG appears at δ = 3.6 ppm, but that from the MeOTr group disappears at approximately 7 ppm. DS_{PEG} was evaluated to be 1.6 from the ^{1}H NMR spectrum of completely propionated **6**. Second, the ester condensation reaction of **6** with the pentynoyl group to yield **2** was monitored using the ^{1}H NMR spectrum exhibiting peaks derived from the protons of the pentynoyl group, AGU, and PEG side chain (Figure S2a): $DS_{pentynoyl}$ was evaluated to be 1.04. The pentynoyl group is introduced mainly at the *O*-6 position preferentially owing to the lower steric hindrance, even though unsubstituted hydroxy groups remain at the *O*-2,3 position. In addition, the ^{13}C NMR spectrum of **2** (Figure S2b) show peaks assigned to C-1, C-6, and carbonyl carbon of pentynoyl group at 102.6 ppm, 62.9 ppm, and 170.9 ppm, respectively, confirming highly regioselective functionalization with the PEG and pentynoyl groups at the *O*-2,3 and *O*-6 positions, respectively.

Finally, copper(I)-catalyzed azide-alkyne cycloaddition (CuAAC click reaction) between **2** and PS-N_3 with different *DP*s was conducted in the presence of $CuSO_4$•$5H_2O$ and ascorbic acid to obtain **1a**–**c**. Figure S3 shows the ^{1}H NMR spectra for **1a**–**c**: the observed peaks are assigned to the protons in the AGU and PEG side chains (δ = 2.70-5.25 ppm) and those in the ethoxycarbonylisopropyl group at the end of the PS chain (δ = 0.8-1.1 ppm; peaks h and j). The amount of PS chains in **1a**–**c** was determined to be 1.0, 1.0 and 1.1 chains per AGU from the peak ratio of these two peaks. Figure S4 shows the SEC profiles detected by UV (λ = 254 nm) for the reaction mixture before (dotted line) and after (solid line) the coupling reaction. The former profile shows only one peak derived from unreacted PS-N_3 since **4** is UV-inactive, while the latter exhibits both a decreased peak for unreacted PS-N_3 and an additional peak corresponding to **1** in the high molecular weight range. By comparing these two peak areas, the *DS* for the PS side chains (DS_{PS}) for **1a**, **1b**, and **1c** was calculated to be 1.0, 1.0 and 1.1, respectively. The matching of DS_{PS} evaluated in different ways supports the notion that the cycloaddition reaction between **2** and PS-N_3 proceeds quantitatively. From the above results, we can conclude that the target heteroBBs **1a**–**c** possess two types of side chains with high density and regioselectivity. The characteristics of the samples are given in Table 1.

Cross-sectional structure of the heterografted bottlebrush determined by SAXS

As one of the key parameters determining the conformation of heteroBB in solution, the cross-sectional structure is discussed based on the value of the cross-sectional radius of gyration (S_c). Here, the electron-density-contrast-weighted S_c value ($\langle S_{c,SAXS}^2 \rangle$) was estimated from the SAXS data for PEG-PS-cellulose **1a–c** and PEG-cellulose **2** in DMF/LiBr according to cross-sectional Guinier plots. Assuming that the bottlebrush adopts a rod-like conformation, $\langle S_{c,SAXS}^2 \rangle$ is described by the following equation in the range of $\langle q^2 \cdot S^2 \rangle \geq 1$ and $q^2 \langle S_{c,SAXS}^2 \rangle \leq 1$:[27,33]

$$\ln[q \cdot I(q)] = A - \frac{1}{2}\langle S_{c,SAXS}{}^2 \rangle q^2 \quad (2)$$

$$q = \frac{4\pi \sin\theta}{\lambda} \quad (3)$$

where q, $I(q)$, 2θ and λ are the scattering vector, scattering intensity, scattering angle and X-ray wavelength, respectively, and A represents a constant factor. Figure 2 shows the cross-sectional Guinier plots of $\ln[q \cdot I(q)]$ versus q^2 from the SAXS profile: the S_c values for **1a**, **1b**, **1c**, and **2** were estimated as 12 nm, 5.4 nm, 3.6 nm and 1.8 nm, respectively, from the slope of the solid line.

Assuming that PEG-PS-cellulose and PEG-cellulose have a constant electron density across the cylinder (homogeneous model), the radius of the bottlebrushes (R) was calculated using the following equation:[27]

$$\langle {S_{\mathrm{c,SAXS}}}^2 \rangle = \frac{R^2}{2} \quad (4)$$

Table 2 lists the R values for PEG-PS-cellulose **1a–c** and PEG-cellulose **2** as well as the previously estimated PS-cellulose **3a–c**. Contrary to expectation, PEG-PS-cellulose has smaller R values compared to the corresponding PS-cellulose with a PS chain of the same molecular weight, although PEG-PS-cellulose possesses additional PEG chains. This suggests that the homogeneous model with a constant electron density inside is inappropriate in these cases. Thus, the contribution of the cellulosic main chain to the SAXS data was explicitly taken into account assuming the core-shell model in which the main chain is surrounded by a shell layer with a different electron density from that in the main chain. This model was applied to the SAXS data obtained for PS-cellulose to determine the density of the cellulosic main chain ($\rho_{\mathrm{cellulose}}$) as the core. As shown in Figure S5, the previously reported experimental data for PS-cellulose **3a–c** are well reproduced by this model with the fitting parameters listed in Table 2: it should be noted that the samples with different $M_{\mathrm{n,PS}}$ were simultaneously analyzed with the same parameters, achieving high accuracy for estimation. The SAXS data for PEG-cellulose and PEG-PS-cellulose were also analyzed using this core-shell model assuming a cellulosic core with the above-determined $\rho_{\mathrm{cellulose}}$ (1.2 g·cm^{-3}) and a homogeneously mixed shell of PEG and PS chains (Figure 3a). Table 2 shows the estimated radius (R) and densities of PEG ($\rho_{\mathrm{solve,PEG}}$) and PS ($\rho_{\mathrm{solve,PS}}$) swollen in DMF/LiBr. The R values for PEG-PS-cellulose are still smaller than those of the

corresponding PS-cellulose with the same $M_{n,PS}$ value. Additionally, the R values are relatively large in comparison with the (contour) length of the PEG chain in the extended state, suggesting that the formation of a homogenous shell layer is disfavored because of the large loss in the conformation entropy of the PEG chain.

Next, inhomogeneity in the shell layer was taken account into the model. Here, the following three models commonly with a cellulosic core with the determined $\rho_{cellulose}$ (1.2 g·cm^{-3}) were examined for PEG-PS-cellulose and PEG-cellulose: coaxially phase-separated models I and II with a core-bilayer-shell structure and a Janus-type phase-separated model with fan-shaped structure, which is a modified model of a Janus cylinder[34], as presented by Walther and coworkers (see Figure S6). In these models, the PEG and PS chains were assumed to be completely phase-separated to form two distinct domains. Unfortunately, the three models were not good enough to reproduce the experimental data obtained for PEG-PS-cellulose and PEG-cellulose (Figure S7, Table S1), especially when $MW_{AGU,PS}$ is close to zero. This suggests that PS and PEG chains can at least partly coexist in the same domain, which is supported by the experimental fact that a homogeneous solution is obtained by mixing linear PS and PEG chains in DMF/LiBr with molecular weights and concentrations corresponding to the case for PEG-PS-cellulose ($\rho_{solve,PS}$ = 0.22 g·cm^{-3}, and $\rho_{solve,PEG}$ = 0.30 g·cm^{-3}, as mentioned below) (see Figure S8a).

Finally, a core-shell-corona model was proposed for PEG-PS-cellulose: the PS and PEG

side chains form a homogeneous shell layer, and one type of side chain protrudes from the shell layer to form a corona layer (Figure 3b). As shown in Figure 4, the experimental data for PEG-PS-cellulose and PEG-cellulose are well reproduced by this core-shell-corona model with the parameters listed in Table 3. The R_{corona} values for PEG-PS-cellulose **1a**, **1b** and **1c** were estimated to be 5.6 nm, 4.0 nm and 3.4 nm, respectively, which are reasonably larger than the R_{shell} values for the corresponding PS-cellulose. We conclude that the core-shell-corona model is the most appropriate for characterizing the cross-sectional structure of PEG-PS-cellulose in DMF/LiBr.

Chain stiffness of the heterografted bottlebrush determined by SEC-MALS

In the previous section, the cross-sectional structure was successfully analyzed, verifying a cylindrical shape with a core-shell-corona structure for PEG-PS-cellulose in DMF/LiBr. Here, we discuss the chain stiffness as another important parameter for characterizing the conformation of bottlebrushes. SEC-MALS measurements were used to obtain data for the molecular-weight dependence of the mean-square radius of gyration $\langle S^2 \rangle$ and, thereby, the stiffness parameter based on the Kratky-Porod wormlike (KP) chain model. Figure 5a shows the SEC profiles in regard to the weight average molecular weight (M_w), $\langle S^2 \rangle$, and polymer mass concentration (c) for PEG-PS-cellulose **1a–c**. Then, these data were converted to the relationship between the $\langle S^2 \rangle$ of the main chain ($\langle S^2 \rangle_M$) and the degree of polymerization of the main chain (DP_M) for analysis with the KP chain model as follows:[28]

$$\langle S^2 \rangle_M = \frac{1}{\lambda^2}\left\{\frac{\lambda L}{6} - \frac{1}{4} + \frac{1}{4\lambda L} - \frac{1}{8\lambda^2 L^2}[1 - exp(-2\lambda L)]\right\} \quad (5)$$

where λ^{-1} and L represent the stiffness parameter and contour length of the main chain of the bottlebrush, respectively. $\langle S^2 \rangle_M$ was calculated using the following equation:[35]

$$\langle S^2 \rangle_M = \langle S^2 \rangle - \langle {S_{c,MALS}}^2 \rangle \quad (6)$$

where $S_{c,MALS}$ is the cross-sectional radius of gyration for MALS, which is calculated using the following equation:

$$\langle {S_{\mathrm{c,MALS}}}^2 \rangle = \frac{R^2}{2} \tag{7}$$

In this case, the R value was set to the value of the outermost layer determined in the previous section. For example, $R = R_{\mathrm{corona}}$ for the core-shell-corona model in the case of PEG-PS-cellulose **1a–c** and $R = R_{\mathrm{shell}}$ for the core-shell model in the case of PS-cellulose **3a–c**. Since the apparent contour length is elongated by side chains near both ends of the main chain, the contour length of the main chain L is estimated using

$$L = \frac{M_{\mathrm{w}}}{M_{\mathrm{L}}} + 2R \tag{8}$$

where M_{L} is the molecular weight per unit contour length of the main chain. M_{L} was calculated based on the assumption that the contour length of the main chain per repeating unit is equal to that of the cellulose crystal (L_{AGU} = 0.52 nm)[36] as follows:

$$\left(\frac{M_0}{M_{\mathrm{L}}}\right)_{\mathbf{1}} = L_{\mathrm{AGU}} \tag{9}$$

where M_0 is the molecular weight per repeat unit. Figure 5b shows the DP_{M} dependence of $\langle S^2 \rangle_{\mathrm{M}}$ for **1a–c**. The theoretical curves for the KP chain model reproduce the experimental data well, indicating that the main-chain conformation of PEG-PS-cellulose is suitably described by the KP chain model. Thus, the estimated stiffness parameter λ^{-1} for PEG-PS-cellulose is listed and compared with that for PS-cellulose, which was determined by reanalyzing the previously reported data using the core-shell model (Figure S9).

The values of λ^{-1} for PEG-PS-cellulose **1a**, **1b**, and **1c** were determined to be larger than

those for the corresponding PS-cellulose **3a**, **3b**, and **3c**, respectively. This can be explained by the fact that PEG-PS-cellulose possesses more side chains than PS-cellulose, as will be discussed in detail later. Nevertheless, the validity of the cross-sectional Guinier approximation for PEG-PS-cellulose **1a–c** is confirmed because these samples have adequately stiff main chains without intramolecular aggregation even in a poor solvent for one side chain.

To discuss the effect of PEG side chains (MW = 750 g·mol^{-1}) at the *O*-2,3 positions on the main-chain stiffness, the relationship between λ^{-1} and DP for PS side chains (m) for PEG-PS-cellulose and PS-cellulose is given in Figure 6. Apparently, with respect to the impact on the stiffness parameter of the main chain, the introduction of two PEG chains (MW = 750 × 2) appears comparable to the elongation due to the increase in the m values from 20 to 60 (see the λ^{-1} values of **1c** and **3a**). Nakamura et al. theoretically derived the following equation concerning the main-chain stiffness of a bottlebrush using first-order perturbation theory:[37]

$$\lambda^{-1} = {\lambda_0}^{-1} + {\lambda_b}^{-1} \tag{10}$$

where λ_0^{-1} is the contribution due to the intrinsic stiffness of the main chain and short-range interaction between the main and side chains, and λ_b^{-1} is derived from the excluded-volume interactions among side chains. Assuming that the side chain takes the Gaussian conformation, λ_b^{-1} is proportional to m^2.[37] Thus, λ^{-1} is given by the following equation:

$$\lambda^{-1} = {\lambda_0}^{-1} + Cm^2 \quad (11)$$

where C is a constant determined by the side chain density, chemical species of the side chain, and solvent quality. The data in Figure 6 can be well fitted by Equation (11) with parameters of λ_0^{-1} = 16 nm and C = 0.0015 ± 0.0002 nm for PEG-PS-cellulose and λ_0^{-1} = 11 nm and C = 0.0015 ± 0.0002 nm for PS-cellulose. It should be noted that the two types of cellulosic bottlebrushes give the same C values. This means that the excluded-volume interactions between the side chains are equivalent despite the substitution of PEG side chains. This may be understood with the already discussed core-shell-corona model of the internal structure of PEG-PS-cellulose, in which the outermost layer dominates. On the other hand, the substitution effect of PEG side chains at the *O*-2,3 position is reflected by a large increase in λ_0^{-1}. This can be interpreted as an increased short-range interaction between the main chain and nearby surrounding shell, in which the substitution of PEG chains results in crowding or jamming of side chains. Additionally, it is noteworthy that the introduction of a bulky substitution at the *O*-2,3 positions effectively suppresses the internal rotation, i.e., the dihedral angle of neighboring AGU units along the cellulose chain. Molecular dynamics simulation work is now under planning to clarify this issue.

Although DMF is a selective solvent (a good solvent for PEG and a poor solvent for PS), PEG-PS-cellulose forms a homogeneous shell layer where PS and PEG side chains coexist. When the selectivity of the solution is increased by adding water, the PS and PEG chains are

expected to undergo intramolecular phase separation (Figure S8b), possibly shifting to the Janus state (Figure S6c). In this case, the dihedral angle of the neighboring AGU units may become distorted via the interaction between the side chains, expectedly leading to a helical conformation for the main chain or helically restricted side chains. This conformation not only enhances fundamental knowledge for cellulosic chemistry but also broadens the diversity of the novel microscale morphology of bottlebrushes in the bulk.

Conclusion

Cellulosic bottlebrushes, PEG-PS-cellulose, with PEG and PS side chains at the *O*-2,3 and *O*-6 positions, respectively, were synthesized by the stepwise grafting-to method via esterification followed by a click reaction. High regioselectivity and substitution of prepared PEG-PS-cellulose and its precursor PEG-cellulose were determined by ^{1}H- and ^{13}C-NMR and SEC measurements. The conformational characteristics of heteroBB, PEG-PS-cellulose, homoBB, and PEG-cellulose in DMF were revealed by assuming a cylindrical shape for the structures, determining the cross-sectional and internal structure as well as the chain stiffness, and comparing these data with that obtained from previously studied PS-cellulose as another homoBB reference. First, the S_c^2 values were evaluated based on a cross-sectional Guinier approximation for the SAXS profiles, followed by discussion of their dependency on the PS chain length and the effect of the introduction of the PEG side chain. Analysis based on several models assuming possibly homogeneous and heterogeneous (phase-separated or multidomain) structures reveals that the PEG-PS-cellulose studied in this article has a cross-sectional core-shell-corona structure, in which the cellulosic core is surrounded by a homogeneous shell layer containing both PS and PEG side chains with an outer corona layer composed of PS: structural parameters including the polymer mass concentration and size of each layer were reasonably determined. Next, the main-chain conformation of cellulosic bottlebrushes was investigated by the SEC-MALS technique and analyzed with the KP

chain model. Then, the estimated stiffness parameter λ^{-1} was described as the sum of two components, λ_0^{-1} and λ_b^{-1}, where the former and latter can be presumably ascribed to the interaction between the main chain and nearby surrounding shell layer and that between PS chains on the adjacent AGUs. It should be noted that the dependence of PS molecular weight on λ_b^{-1} was found to be almost the same with and without PEG chains, suggesting that the introduction of relatively thin and short PEG chains mainly and effectively contributes to λ_0^{-1} owing to side chain crowding in the shell. This is considered the conformational characteristic of cellulosic bottlebrushes, in which rigid AGU components are connected via glycosidic bonds. Their stiffness can be understood by the distribution of the dihedral angle affected by, e.g., the substitution of PEG chains at the *O*-2,3 position.

Acknowledgment

High-resolution 600 MHz and 800 MHz NMR spectra were acquired with an NMR spectrometer in the Joint Usage/Research Center (JURC) at the Institute for Chemical Research, Kyoto University. Synchrotron SAXS experiments were performed at BL40B2 (Proposal Nos. 2016B1208 and 2017B1727) in SPring-8 with the approval of the Japan Synchrotron Radiation Research Institute (JASRI). The authors thank Dr. Noboru Ohta (JASRI/SPring-8) for assistance with the experiments carried out using the BL40B2 beamline. This work was supported by a Grant-in-Aid for Challenging Exploratory Research (No. 25620175) and a Grant-in-Aid for Young Scientists (B) (No. 16K17914) from the Ministry of Education, Culture, Sports, and Technology (MEXT) in Japan.

References

1. Xie G, Martinez MR, Olszewski M, Sheiko SS, Matyjaszewski K. Molecular Bottlebrushes as Novel Materials. Biomacromolecules. 2019;20(1):27-54.

2. Tsukahara Y, Miyata M, Senoo K, Yoshimoto N, Kaeriyama K. Mesomorphic Phase Formation of Poly (macromonomer)s of Polystyrene Macromonomers. Polym Adv Technol. 2000;11(5):210-218.

3. Daniel WF, Burdynska J, Vatankhah-Varnoosfaderani M, et al. Solvent-Free, Supersoft and Superelastic Bottlebrush Melts and Networks. Nat Mater. 2016;15(2):183-189.

4. Altay E, Nykypanchuk D, Rzayev J. Mesoporous Polymer Frameworks from End-Reactive Bottlebrush Copolymers. ACS Nano. 2017;11(8):8207-8214.

5. Liu X. Surface Forces between Bottlebrush Polymer Layers. Curr Opin Colloid Interface Sci. 2020;47:16-26.

6. Tu S, Choudhury CK, Luzinov I, Kuksenok O. Recent advances towards applications of molecular bottlebrushes and their conjugates. Curr Opin Solid State Mater Sci. 2019;23(1):50-61.

7. Kinose Y, Sakakibara K, Sato O, Tsujii Y. Near-Zero Azimuthal Anchoring of Liquid Crystals Assisted by Viscoelastic Bottlebrush Polymers. ACS Appl Polym Mater. 2021;3(5):2618-2625.

8. Yoshikawa C, Sakakibara K, Nonsuwan P, Yamazaki T, Tsujii Y. Nonbiofouling Coatings Using Bottlebrushes with Concentrated Polymer Brush Architecture. Biomacromolecules. 2021;22(6):2505-2514.

9. Chen K, Hu X, Zhu N, Guo K. Design, Synthesis, and Self-Assembly of Janus Bottlebrush Polymers. Macromol Rapid Commun. 2020;41(20):2000357.

10. Le AN, Liang R, Zhong M. Synthesis and Self-Assembly of Mixed-Graft Block Copolymers. Chemistry. 2019;25(35):8177-8189.

11. Xie G, Krys P, Tilton RD, Matyjaszewski K. Heterografted Molecular Brushes as Stabilizers for Water-in-Oil Emulsions. Macromolecules. 2017;50(7):2942-2950.

12. Li Y, Zou J, Das BP, Tsianou M, Cheng C. Well-Defined Amphiphilic Double-Brush Copolymers and Their Performance as Emulsion Surfactants. Macromolecules. 2012;45(11):4623-4629.

13. Palacios-Hernandez T, Luo H, Garcia EA, Pacheco LA, Herrera-Alonso M. Nanoparticles from Amphiphilic Heterografted Macromolecular Brushes with Short Backbones. Macromolecules. 2018;51(8):2831-2837.

14. Chang HY, Lin YL, Sheng YJ, Tsao HK. Multilayered Polymersome Formed by Amphiphilic Asymmetric Macromolecular Brushes. Macromolecules. 2012;45(11):4778-4789.

15. Nam J, Kim Y, Kim JG, Seo M. Self-Assembly of Monolayer Vesicles via Backbone-Shiftable Synthesis of Janus Core–Shell Bottlebrush Polymer. Macromolecules. 2019;52(24):9484-9494.

16. Guo ZH, Le AN, Feng X, et al. Janus Graft Block Copolymers: Design of a Polymer Architecture for Independently Tuned Nanostructures and Polymer Properties. Angew Chem, Int Ed. 2018;57(28):8493-8497.

17. Kawamoto K, Zhong M, Gadelrab KR, et al. Graft-through Synthesis and Assembly of Janus Bottlebrush Polymers from A-Branch-B Diblock Macromonomers. J Am Chem Soc. 2016;138(36):11501-11504.

18. Stepanyan R, Subbotin A, ten Brinke G. Comb Copolymer Brush with Chemically Different Side Chains. Macromolecules. 2002;35(14):5640-5648.

19. Hsu H-P, Paul W, Binder K. Intramolecular Phase Separation of Copolymer "Bottle Brushes": No Sharp Phase Transition but a Tunable Length Scale. Europhys Lett. 2006;76(3):526-532.

20. Theodorakis PE, Paul W, Binder K. Analysis of the Cluster Formation in Two-Component Cylindrical Bottle-Brush Polymers under Poor Solvent Conditions: a Simulation Study. Eur Phys J E: Soft Matter Biol Phys. 2011;34(5):52.

21. de Jong J, ten Brinke G. Conformational Aspects and Intramolecular Phase Separation of

Alternating Copolymacromonomers: A Computer Simulation Study. Macromol Theory Simul. 2004;13(4):318-327.

22. Kinose Y, Sakakibara K, Ogawa H, Tsujii Y. *Main-Chain Stiffness of Cellulosic Bottlebrushes with Polystyrene Side Chains Introduced Regioselectively at the O*-6 Position. Macromolecules. 2019;52(22):8733-8740.

23. Sakakibara K, Ishida H, Kinose Y, Tsujii Y. Regioselective synthesis of cellulosic janus bottlebrushes with polystyrene and poly (ε-caprolactone) side chains and their solid-state microphase separation. Cellulose. 2021;28(11):6857-6868.

24. Sheiko SS, Borisov OV, Prokhorova SA, Moller M. Cylindrical Molecular Brushes under Poor Solvent Conditions: Microscopic Observation and Scaling Analysis. Eur Phys J E. 2004;13(2):125-131.

25. Grulke EA. Solubility Parameter Values. In: Brandrup J, Immergut EH, Grulke EA, editors. Polymer Handbook. 4th ed. New York: Wiley; 1999:VI-675 - VI-714.

26. Sakakibara K, Kinose Y, Tsujii Y. Synthesis of Cellulosic Bottlebrushes with Regioselectively Substituted Side Chains and Their Self-assembly. In: Rosenau T, Potthast A, Hell J, editors. Cellulose Science and Technology: Chemistry, Analysis, and Applications. New York: Wiley; 2019:49-65.

27. Glatter O, Kratky O. Small Angle X-ray Scattering. London: Academic Press; 1982.

28. Benoit H, Doty P. Light Scattering from Non-Gaussian Chains. J Phys Chem. 1953;57(9):958-963.

29. Benoit H, Froelich D. Application of Light Scattering to Copolymers. In: Huglin MB, editor. Huglin MB, trans. Light Scattering from Polymer Solutions. London and New York: Academic Press; 1972:467-501.

30. Gömez JAC, Erler UW, Klemm DO. 4-Methoxy Substituted Trityl Groups in 6-O Protection of Cellulose: Homogeneous Synthesis, Characterization, Detritylation. Macromol Chem Phys. 1996;197(3):953-964.

31. Yue Z, Cowie JMG. Preparation and Chiroptical Properties of a Regioselectively Substituted Cellulose Ether with PEO Side Chains. Macromolecules. 2002;35(17):6572-6577.

32. Matyjaszewski K, Nakagawa Y, Gaynor SG. Synthesis of Well-Defined Azido and Amino End-Functionalized Polystyrene by Atom Transfer Radical Polymerization. Macromol Rapid Commun. 1997;18(12):1057-1066 (Article).

33. Wataoka I, Kobayashi K, Kajiwara K. Effect of the Carbohydrate Side-Chain on the Conformation of a Glycoconjugate Polystyrene in Aqueous Solution. Carbohydr Res. 2005;340(5):989-995.

34. Walther A, Drechsler M, Rosenfeldt S, et al. Self-Assembly of Janus Cylinders into

Hierarchical Superstructures. J Am Chem Soc. 2009;131(13):4720-4728.

35. Yamakawa H, Yoshizaki T. Helical Wormlike Chains in Polymer Solutions. 2nd ed. Berlin: Springer, Berlin Heidelberg; 2016.

36. Sugiyama J, Vuong R, Chanzy H. Electron Diffraction Study on the Two Crystalline Phases Occurring in Native Cellulose from an Algal Cell Wall. Macromolecules. 1991;24(14):4168-4175.

37. Nakamura Y, Norisuye T. Backbone Stiffness of Comb-Branched Polymers. Polym J. 2001;33(11):874-878.

Figure legends

Graphical abstract. Cellulosic bottlebrush regioselectively possessing poly(ethylene glycol) (PEG) and polystyrene (PS) side chains (PEG-PS-cellulose) was synthesized, and its secondary structure in dilute solution was investigated with SAXS and SEC-MALS. The relationship between the cross-sectional mean squared radius of gyration ($\langle S_c^2 \rangle$) and molecular weight of PS chain (MW_{PS}) showed that PEG-PS-cellulose has a core-shell-corona structure in cross section. The dependency of main-chain stiffness (λ^{-1}) on MW_{PS} was discussed on the basis of the interactions of the PS and PEG side chains as well as the restricted rotation of the cellulosic main chain.

Figure. 1. Chemical structures of heteroBBs (PEG-PS-cellulose **1**) and homoBBs (PEG-cellulose **2** and PS-cellulose **3**).

Scheme 1. Synthesis of PEG-PS-cellulose **1** and its precursor, PEG-cellulose **2**.[a]

[a] Reagents, conditions and yields: (a) PEG-I, NaOH, DMSO, 50 °C, 4 d, 75%; (b) HCl, H_2O, THF, rt, 5 h, 88%; (c) pentynoic acid, EDC•HCl, DMF, rt, 1 d→50 °C, 2 d, 98%; (d) PS-N_3 (DP_n = 60 (for **1a**), 30 (for **1b**), 20 (for **1c**)), $CuSO_4$•$5H_2O$, ascorbic acid, DMF, 60 °C, 2 d, 75% (**1a**), 76% (**1b**), 75% (**1c**).

Figure 2. Cross-sectional Guinier plots for bottlebrushes; **1a, 1b** and **1c** (red, blue and green circles); **2** (purple circle); **3a, 3b** and **3c** (red, blue and green squares). The solid lines represent the increment of the cross-sectional Guinier approximation. Adapted with permission from Ref. No.22. Copyright 2011. American Chemical Society.

Figure 3. Schematic illustration and radial density diagram of the cross-sectional structure for the core-shell model (a) and core-shell-corona model (b) for PEG-PS-cellulose **1**. Gray: cellulosic backbone; orange: PS domain; blue: PEG domain.

Figure 4. The relationship between $\langle S_{c,SAXS}^2 \rangle$ and $MW_{AGU,PS}$ for PEG-PS-cellulose (**1a–c**) and PEG-cellulose (**2**). The red curve represents the theoretical curve for the core-shell-corona model

for PEG-PS-cellulose illustrated in Figure 3b ($\rho_{cellulose}$ = 1.2 g·cm^{-3}, $\rho_{solve,PS}$ = 0.22 g·cm^{-3} and $\rho_{solve,PEG}$ = 0.30 g·cm^{-3}).

Figure 5. Elution-volume dependence of the weight-average molecular weight M_w (blue circles), mean-square radius of gyration $\langle S^2 \rangle$ (red circles) and polymer mass concentration c (solid line) (a), and DP_M chain dependence of $\langle S^2 \rangle_M$ in DMF/LiBr for PEG-PS-cellulose (b) for **1a–c**. The red lines in (b) represent the theoretical curves for the unperturbed KP chain.

Figure 6. The dependence of λ^{-1} on the DP_n of the side chains (m) for **1** and **3** in DMF/LiBr (red and blue circles, respectively). The red and blue solid lines represent theoretical curves for **1** and **3**, respectively.

Graphical abstract

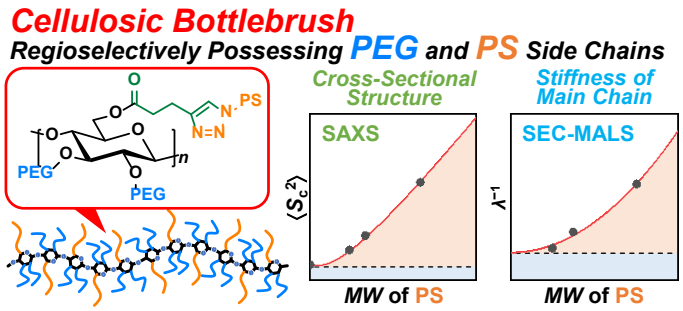

Figure. 1

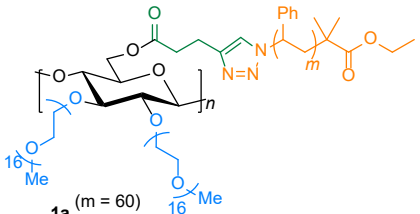

1a (m = 60)
1b (m = 30)
1c (m = 20)

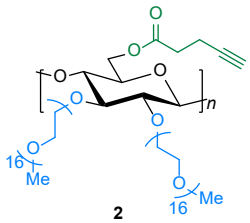

2

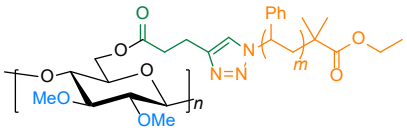

3a (m = 60)
3b (m = 30)
3c (m = 20)

Scheme 1

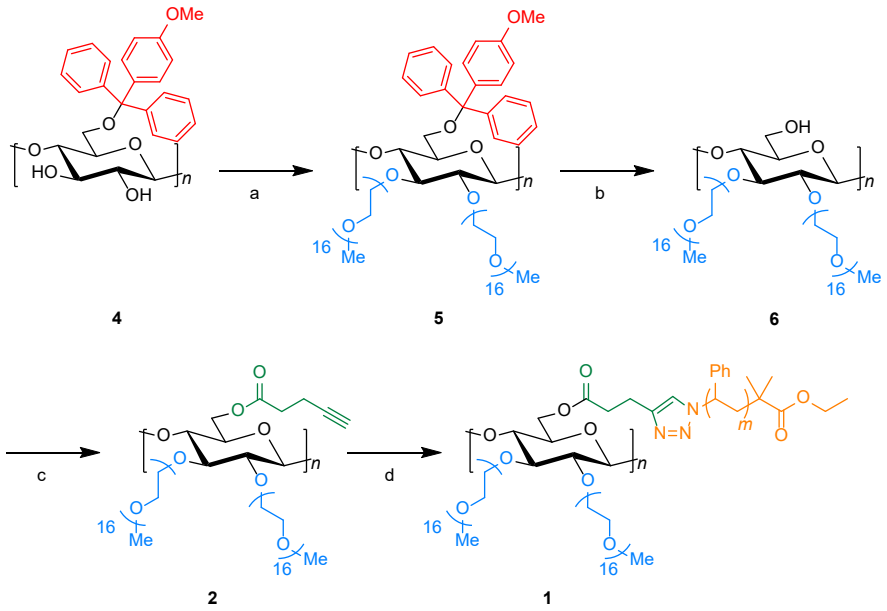

Figure 2

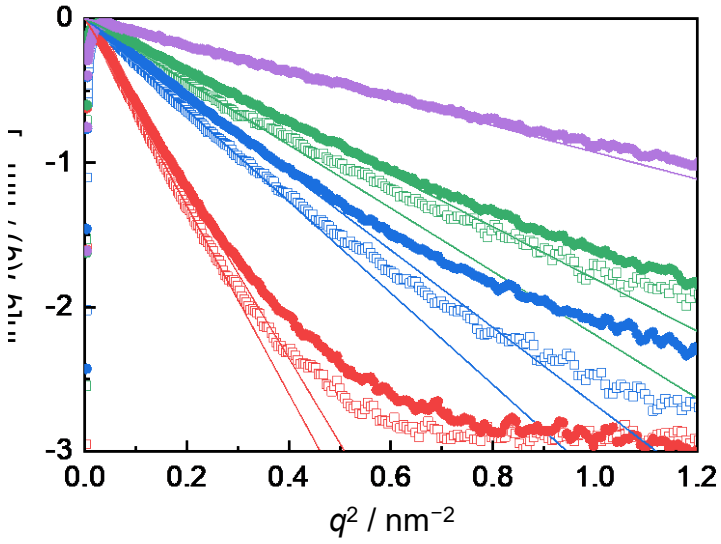

Figure 3

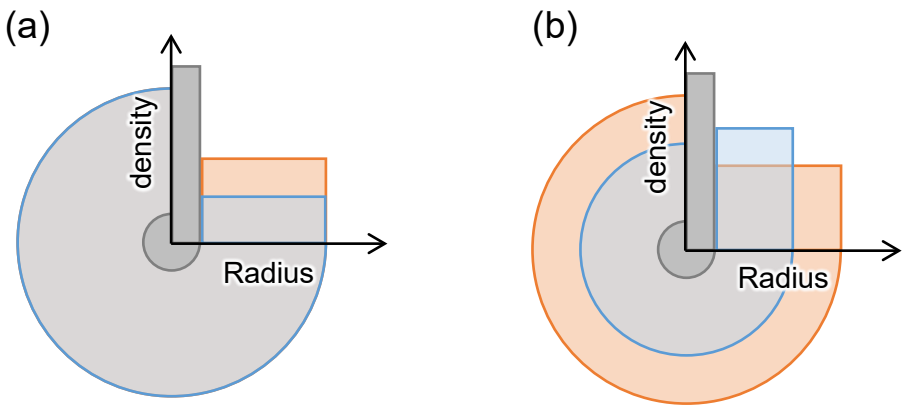

Figure 4

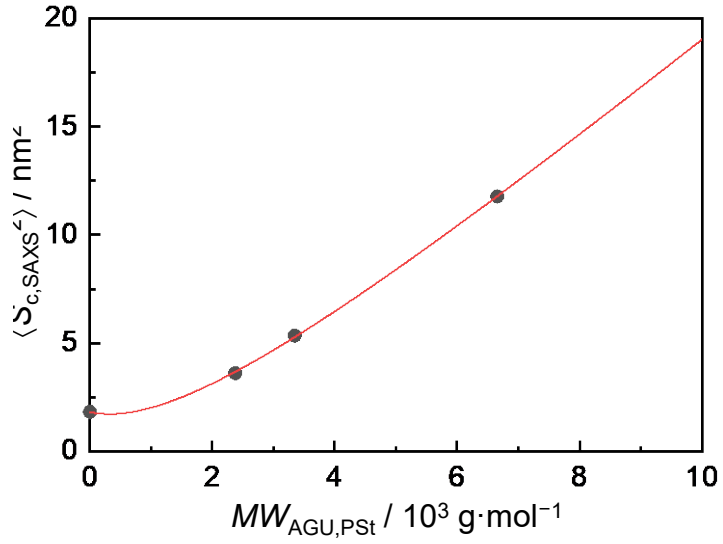
20
15
10
5
0
0
2
4
6
8
10
$\langle s_{c,SAXS}^2 \rangle$ / nm²
$MW_{AGU,PSt}$ / 10^3 g·mol^{-1}

Figure 5

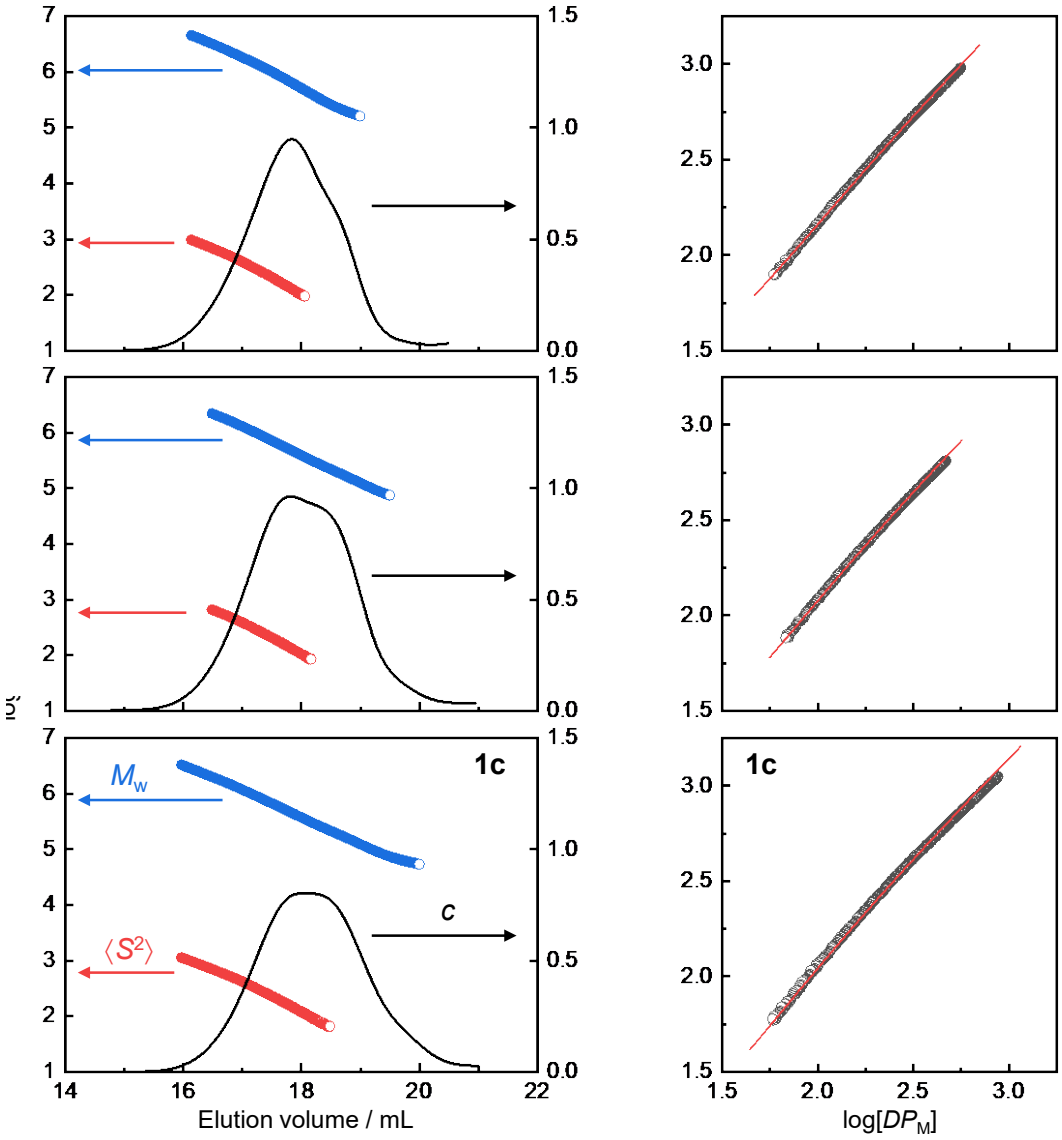

Figure 6

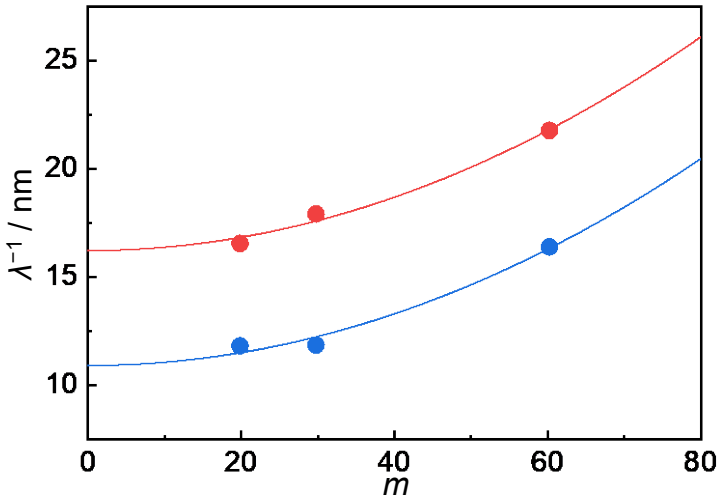

Table 1. Characteristics of cellulosic bottlebrushes **1**, **2** and **3**.

		Sample	DS_{PEG}	DS_{PS}	$M_{n,PS}$/g·mol^{-1}	M_0[a]/g·mol^{-1}	$w_{backbone}$[b]	w_{PEG}[b]	w_{PS}[b]	dn/dc[c]/g·mol^{-1}	M_w[d]/g·mol^{-1}	DP_M[d]	$Đ$[d]	$\langle S_{c,SAXS}^2 \rangle^f$/nm^2
heteroBB	PEG-PS-cellulose	**1a**	1.6	1.0	6.4×10^3	8.1×10^3	0.03	0.14	0.83	0.139	9.7×10^5	1.2×10^2	2.3	12
		1b	1.6	1.0	3.3×10^3	4.7×10^3	0.05	0.24	0.71	0.126	6.1×10^5	1.3×10^2	2.4	5.4
		1c	1.6	1.1	2.2×10^3	3.8×10^3	0.06	0.31	0.63	0.117	4.8×10^5	1.3×10^2	2.4	3.6
	PEG-cellulose	**2**	1.6	—	—	1.4×10^3	—	—	—	—	6.2×10^4[e]	4.4×10^2[e]	1.5[e]	1.8
homoBB	PS-cellulose[e]	**3a**[g]	—	1.1	6.4×10^3	7.4×10^3	0.04	—	0.96	0.154	8.1×10^5	1.1×10^2	1.6	13
		3b[g]	—	1.1	3.3×10^3	3.8×10^3	0.07	—	0.93	0.150	4.6×10^5	1.2×10^2	1.7	6.4
		3c[g]	—	1.2	2.2×10^3	2.9×10^3	0.10	—	0.90	0.148	3.2×10^5	1.1×10^2	1.7	4.3

[a]Average molecular weight per AGU. [b]Weight fraction of the main chain and PEG and PS side chains. [c]Refractive index increment calculated from equation 1. [d]Determined by SEC-MALS in DMF/LiBr. [e]Determined by SEC with PMMA standard with the cross-sectional Guinier approximation. [f]Mean-square radius of gyration determined from the SAXS profile. [g]Adapted with permission from Ref. No.22. Copyright 2011. American Chemical Society.

Table 2. Model parameters for cellulosic bottlebrushes **1**, **2** and **3**.

		Homogeneous model	Core-shell model					Core-shell-corona model					
		R /nm	$\rho_{cellulose}$ / g·cm^{-3}	$\rho_{solve,PS}$ / g·cm^{-3}	$\rho_{solve,PEG}$ / g·cm^{-3}	R_{core} / nm	R_{shell} /nm	$\rho_{cellulose}$ / g·cm^{-3}	$\rho_{solve,PS}$ / g·cm^{-3}	$\rho_{solve,PEG}$ / g·cm^{-3}	R_{core} / nm	R_{shell} / nm	R_{corona} /nm
PEG-PS-cellulose	**1a**	4.9	1.2[b]	0.28[c]	0.048[c]	0.46[d]	5.0	1.2[b]	0.22	0.30	0.46[d]	2.0[f]	5.6[f]
	1b	3.3		0.30[c]	0.10[c]		3.4					2.0[f]	4.0[f]
	1c	2.7		0.32[c]	0.16[c]		2.7					2.0[f]	3.4[f]
PEG-cellulose	**2**	1.9		—	0.29[c]		2.0		—			2.0[f]	—
PS-cellulose	**3a**	5.1[a]	1.2	0.26	—	0.50[d]	5.3[e]	—	—	—	—	—	—
	3b	3.6[a]			—		3.8[e]	—	—	—	—	—	—
	3c	2.9[a]			—		3.2[e]	—	—	—	—	—	—

[a] Data in ref. 22. [b] Constant parameter. [c] Depending on R_{shell}. [d] Depending on $\rho_{cellulose.}$ [e] Depending on $\rho_{cellulose}$ and $\rho_{solve,PS}$. [f] Depending on $\rho_{cellulose}$, $_{solve,PS}$ and $\rho_{solve,PEG}$

Table 3. Stiffness parameters for PEO-PS-cellulose **1** and PS-cellulose **3**.

Sample		DP_n of PS-side chain (m)	λ^{-1}/nm
PEG-PS-cellulose	**1a**	60	22
	1b	30	18
	1c	20	17
PS-cellulose[a]	**3a**	60	16
	3b	30	12
	3c	20	12

[a] From reanalysis of the data in ref. 22 using the core-shell model.